Indian Journal of Pure & Applied Physics
Vol. 64, July 2026, pp. 796-802
DOI: 10.56042/ijpap.v64i7.30439

Impact of Source Contact Engineering on Memory Window Enhancement in PVDF/ZnO Ferroelectric Thin-Film Transistors

Nitin Chandravanshi, Aditya Maithani, Arun K Singh, Divya Dhawan & Deepak K Sharma*

Department of Electronics and Communication Engineering, Punjab Engineering College (Deemed to be University), Chandigarh 160 012, India

Received: 6th April 2026; accepted: 15th May 2026

In this work, memory window (MW) modulation in bottom gate ZnO/PVDF ferroelectric thin-film transistors (FeTFTs) is studied using Schottky and Ohmic source/drain contact configurations using a TCAD simulation framework. The influence of contact dependent carrier injection and ZnO background electron concentration ranging from 10^{15} to 10^{17} cm^{-3} on polarization screening and hysteresis properties is comprehensively examined under a transient gate dual sweep voltage of 0 to 20 V with a total pulse duration of 2 μs. Devices with Schottky contacts show clearly defined hysteresis loops in input characteristics with MW within 2.86 and 3.69 V, whereas devices with Ohmic contacts indicate significantly lower MW between 0.21 and 0.22 V, which is attributed to increased electrostatic charge screening and unrestricted carrier supply. Further the observed behavior is analyzed using carrier concentration distribution analysis plots which shows that reduced carrier concentration at the Schottky interface enhances polarization induced potential modulation, while higher carrier availability in Ohmic devices lowers this effect. In ZnO/PVDF FeTFT platforms, this work clearly shows that source/drain contact engineering is a governing mechanism for controlling polarization charge screening and improving ferroelectric memory performance.

Keywords: TCAD, ZnO TFT, PVDF, Ferroelectric memory, Memory window, Schottky and ohmic contact

1 Introduction

Thin film transistors (TFTs) are widely used in applications like flexible electronics, flat panel displays, and sensors, and they are essential to large area electronic systems. Unlike conventional bulk MOSFETs, TFTs employ thin semiconductor layers deposited on insulating substrates, enabling the fabrication of large scale, mechanically flexible platforms. Because of this ability, TFT technology is now a crucial part of both new flexible electronic systems and contemporary display backplanes[1,2]. Zinc oxide (ZnO) is a semiconductor material that has garnered a lot of interest as a TFT channel material because of its wide bandgap, optical transparency, and suitability for low temperature fabrication processes[3-6]. Additionally, interface engineering with high-k gate dielectrics like Al_2O_3 can improve device performance and stability in ZnO TFTs by lowering interface trap density at the semiconductor dielectric interface and improving gate electrostatic control[7,8].

By adding ferroelectric materials to the gate stack of TFTs, polarization induced modulation of the channel surface potential allows for non-volatile memory functionality. Ferroelectric field effect transistors (FeFETs) utilize the remanent polarization of the ferroelectric layer to produce two stable threshold voltage states, and the separation between these states defines the memory window (MW)[9,10]. Among different ferroelectric materials, poly(vinylidene fluoride) (PVDF) and its copolymers have attracted a lot of interest due to their strong remanent polarization, mechanical flexibility, and suitability for low temperature processing techniques[11,12]. ZnO/P(VDF-TrFE) based ferroelectric TFTs have demonstrated promising hysteresis behavior and non-volatile memory characteristics[13,14]. The MW in such devices originates from the electrostatic coupling between ferroelectric polarization and the semiconductor channel, where polarization induced bound charges modulate the channel surface potential and shifts the threshold voltage[15,16]. However, this modulation strongly depends on the availability of mobile carriers in the semiconductor channel that can compensate the polarization charges, and insufficient carrier supply can suppress polarization switching and reduce the achievable MW[17,18].

Since carrier supply in TFT devices is strongly influenced by the source/drain contacts and channel carrier concentration, the contact configuration plays

*Corresponding author: E-mail: deepaksk@pec.edu.in

a critical role in determining polarization screening and memory characteristics[19]. In particular, Schottky contacts can restrict carrier injection into the channel, whereas Ohmic contacts allow efficient carrier transport from the electrodes, thereby influencing the degree of polarization charge screening at the ferroelectric interface[20]. In this work, a systematic TCAD investigation of bottom gate ZnO/PVDF ferroelectric TFTs is performed to analyze the influence of source/drain contact configuration and ZnO background electron concentration (10^{15}–10^{17} cm^{-3}) on MW behavior under transient polarization switching. This study provides the first comprehensive examination of contact-controlled polarization screening in ZnO/PVDF ferroelectric TFTs. It also identifies the role of carrier injection limited hysteresis in Schottky contact devices and demonstrates that Schottky contacts improve the memory window in oxide ferroelectric TFTs by suppressing carrier mediated screening of polarization charges.

2 Device Structure and Simulation Methodology

The simulated bottom gate ZnO/PVDF ferroelectric thin film transistor (FeTFT) structure is illustrated in Fig. 1. The device consists of an aluminum (Al) bottom gate electrode, a ferroelectric poly(vinylidene fluoride) (PVDF) layer, an ultra-thin Al_2O_3 interfacial layer to improve the interface, an n-type ZnO semiconductor channel, and palladium (Pd) source and drain electrodes. Palladium (Pd) source/drain electrodes possessing a work function of 5.1 eV were utilized, the electron affinity of ZnO is kept as 4.4 eV, that results in an electron Schottky barrier of roughly 0.7 eV at the Pd/ZnO contact. The interface was considered perfect, excluding any contributions from interface trap-assisted pinning effects. This configuration represents a typical bottom

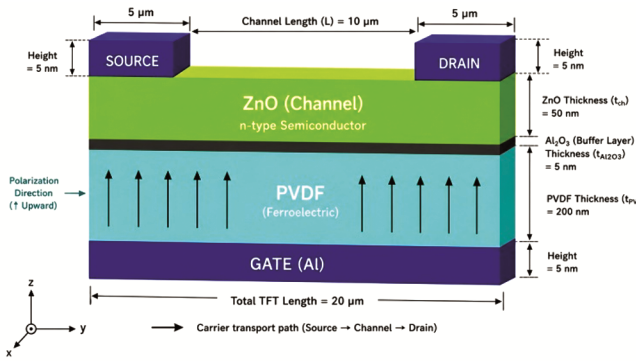

Fig. 1 — Bottom gate ZnO/PVDF ferroelectric TFT structure with Al_2O_3 buffer layer

gate ferroelectric TFT architecture in which the ferroelectric layer is integrated within the gate stack to modulate the electrostatics of the semiconductor channel[14,22].

For the source and drain electrodes, palladium was chosen because it has a work function of about 5.1 eV, which allows for controlled Schottky barrier formation at the metal ZnO interface[19]. To systematically study the impact of carrier concentration on polarization screening and memory window behavior, the ZnO channel was modeled as uniformly n-type with background electron concentrations of 1×10^{17}, 1×10^{16} and 1×10^{15} cm^{-3}. During gate voltage sweeps, the PVDF ferroelectric layer's remanent polarization modifies the ZnO channel's surface potential, resulting in hysteresis or threshold voltage shifts[10]. An ultra-thin Al_2O_3 buffer layer was introduced between the ZnO channel and the PVDF layer to improve the interface quality and reduce interface trap effects. This interfacial layer also helps in stabilizing the ferroelectric semiconductor interface and suppress depolarization effects, consistent with previously reported ZnO/P(VDF-TrFE) interface engineering approaches[13,23]. Two different source and drain contact configurations were investigated to analyze the influence of carrier injection on ferroelectric polarization screening. In the first case, a finite electron barrier height was defined to create Schottky contacts at the Pd/ZnO interface. In this scenario, tunneling and thermionic emission are the main ways that carriers are transported across the metal semiconductor interface[19]. The Silvaco ATLAS simulator's Universal Schottky Tunneling (ust) model was activated in order to precisely represent these processes. The Schottky barrier limits the compensation of polarization induced bound charges at the ZnO/PVDF interface by preventing electron injection from the source and drain electrodes into the ZnO channel[18]. In the second case, the source and drain terminals had ideal Ohmic contacts. In this configuration, carriers can be injected into the ZnO channel without significant energy barriers, enabling efficient carrier supply from the metal electrodes. The resulting higher carrier concentration near the channel interface enhances electrostatic screening of ferroelectric polarization charges, which significantly influences the hysteresis behavior and reduces the achievable memory window[15]. All device simulations were performed using the Silvaco ATLAS TCAD simulator under a two-dimensional drift–diffusion

transport framework[25]. In this framework, the coupled Poisson equation and carrier continuity equations are solved self consistently to determine the electrostatic potential distribution and carrier transport within the device structure. Shockley–Read–Hall recombination and Auger recombination were included to account for carrier recombination mechanisms. Field dependent mobility was incorporated to capture the influence of high electric fields on carrier transport, while Fermi–Dirac statistics were used to accurately describe carrier distribution in the semiconductor. For simulations involving Schottky contacts, the Universal Schottky Tunneling (ust) model was activated to account for thermionic emission and barrier tunneling at the metal semiconductor interface. All simulations were performed at a room temperature of 300 K. The ferroelectric behavior of the PVDF layer was modeled using the Silvaco ATLAS ferro material model[26], which describes ferroelectric polarization using a nonlinear field dependent formulation[10,21]. In this approach, the electric displacement consists of a linear dielectric contribution and a nonlinear polarization component governed by parameters such as saturation polarization, remanent polarization, coercive field, and ferroelectric permittivity, which were defined to reproduce the characteristic polarization electric field hysteresis behavior of PVDF based ferroelectric films[24]. To capture the dynamic switching behavior of the ferroelectric layer, transient simulations were performed using a triangular gate voltage excitation applied to the bottom gate electrode, consisting of a positive sweep from 0 V to +20 V followed by a reverse sweep back to 0 V with a total pulse duration of 2 μs. During the simulation, the drain voltage was maintained at a constant bias of 5 V to extract the input characteristics. The hysteresis observed in the drain current versus gate voltage characteristics originates from polarization switching in the PVDF layer, and the memory window (MW) was extracted from the separation between the threshold voltages obtained during the forward and reverse sweeps. This transient approach enables realistic modeling of polarization dynamics and provides an accurate estimation of the memory window under practical operating conditions.

3 Results and Discussion

3.1 Input Characteristics and Memory Window Extraction

The input characteristics (Id–Vg) were extracted during the triangular transient gate sweep from 0 V to +20 V and back to 0 V with a total pulse duration of 2 μs. The simulated transfer characteristics exhibit clear gate-controlled modulation of drain current with ON current for Schottky source device during forward sweep varies from 0.05 mA to 0.07 mA for ZnO background concentrations from 10^{15} to 10^{17}/cc. The memory window (MW) was defined as the threshold voltage separation between the programmed and erased states[10].

Figures 2 (a)–(c) shows the input characteristics of the Schottky contact devices. Pronounced hysteresis loops are clearly observed for all doping levels, indicating strong polarization channel coupling during transient switching. A systematic increase in MW is observed as the ZnO background electron concentration decreases. The MW increases from 2.86 V at 1×10^{17} cm^{-3} to 3.69 V at 1×10^{15} cm^{-3}. The increase in MW with decreasing ZnO electron concentration can be attributed to the electrostatic interaction between the ferroelectric polarization charges in PVDF and the depletion region formed at the metal-ZnO Schottky interface[19]. As the carrier concentration in ZnO decreases, the depletion width at the Schottky junction expands, and the density of mobile carriers adjacent to the interface declines. As a result, the electrostatic screening of the ferroelectric polarization charges at the PVDF/ZnO contact reduces resulting in the increase in polarization

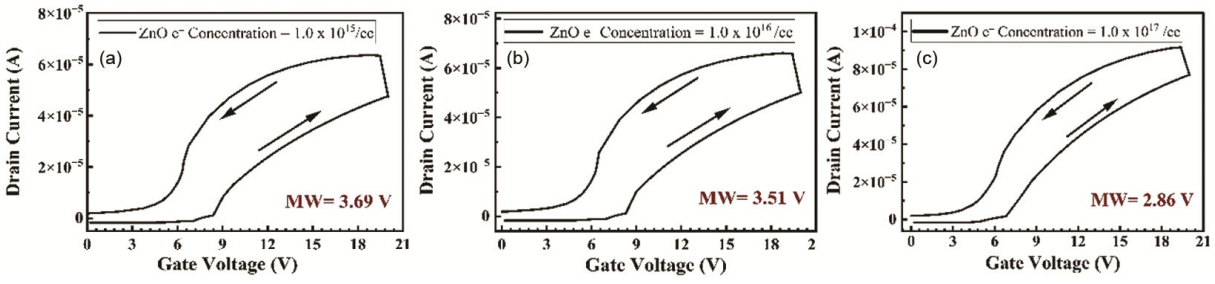

Fig. 2 — Input characteristics of Schottky contact ZnO/PVDF FeTFTs under triangular transient gate sweep for ZnO electron concentrations of (a) 1×10^{15}, (b) 1×10^{16}; and (c) 1×10^{17} cm^{-3}

induced electric field penetration into the ZnO region which more efficiently influences the electrostatics and band bending at the metal semiconductor interface. The orientation of polarization influences the bound charges at the PVDF/ZnO interface, hence modifying the local electrostatic potential and effectively altering the Schottky barrier height. The alteration of the Schottky barrier generated by polarization subsequently affects carrier injection from the metal contact into the ZnO channel, leading to an increased difference in threshold voltage between the two polarization states and, consequently, a broader memory window[18]. On further reducing the background electron concentration; the electrostatic coupling between the ferroelectric polarization and the semiconductor channel does not enhance significantly, thus resulting in limited increase in the memory window.

Figure 3 (a)–(c) shows the input characteristics of the Ohmic contact devices under identical transient conditions. The simulated transfer characteristics exhibit clear gate-controlled modulation of drain current with ON current for ohmic source device during forward sweep varies from 0.69 mA to 0.73 mA for ZnO background concentrations from 10^{15} to 10^{17}/cc. The hysteresis loops are significantly suppressed compared to the Schottky contact configuration. The extracted MW remains limited to approximately 0.21–0.22 V across all doping levels, showing only weak dependence on carrier concentration. Under the present condition, the metal semiconductor interface provides a negligible barrier for carrier injection, and carrier transport is therefore mainly governed by the conductivity of the ZnO channel rather than by contact barrier modulation. The polarization charges at the PVDF/ZnO interface are efficiently screened by the high density of free carriers supplied by the Ohmic contacts and the relatively conductive channel[15]. As a result, the polarization field has only a weak influence on the band bending at the metal semiconductor interface and therefore on carrier injection in the device. Consequently, the shift in threshold voltage between the two polarization states remains small, leading to a limited MW of approximately 0.2 V and minimal dependence on ZnO carrier concentration. Table 1 summarizes the extracted MW values for both contact configurations, demonstrating the clear distinctions between the two device structures. In Schottky contact devices, the MW increases from 2.86 V to 3.69 V when the ZnO electron concentration drops from 1×10^{17} to 1×10^{15} cm^{-3}. On the other hand, Ohmic contact devices shows a much smaller MW of about 0.21–0.22 V with minimal dependence on carrier concentration. The observed memory window highlights the critical role of contact-controlled carrier injection in determining the memory characteristics of ZnO/PVDF FeTFTs.

3.2 Electron Concentration Distribution Analysis

To further understand the role of carrier injection and polarization screening, electron concentration contour plots were analyzed at different gate bias conditions without any initial conditions of gate bias. Figure 4 (a) and (b) show the electron concentration distributions for the Schottky contact device at low and high gate bias, respectively, while Fig. 4 (c) and (d) present the corresponding distributions for the Ohmic contact device at low and high gate bias for an

Table 1 — Extracted memory window comparison for different ZnO electron concentrations

ZnO Electron Conc. (cm^{-3})	Schottky MW (V)	Ohmic MW (V)
1×10^{17}	2.86	0.210
1×10^{16}	3.51	0.212
1×10^{15}	3.69	0.220

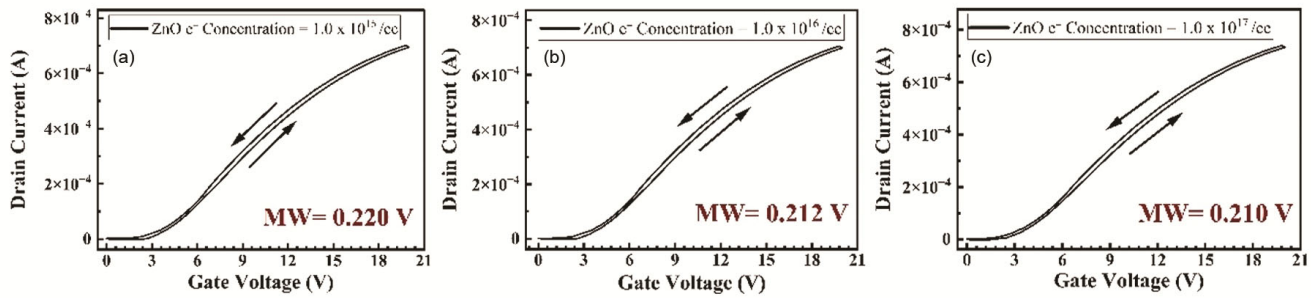

Fig. 3 — Input characteristics of Ohmic contact ZnO/PVDF FeTFTs under triangular transient gate sweep for ZnO electron concentrations of (a) 1×10^{15}, (b) 1×10^{16} and (c) 1×10^{17} cm^{-3}

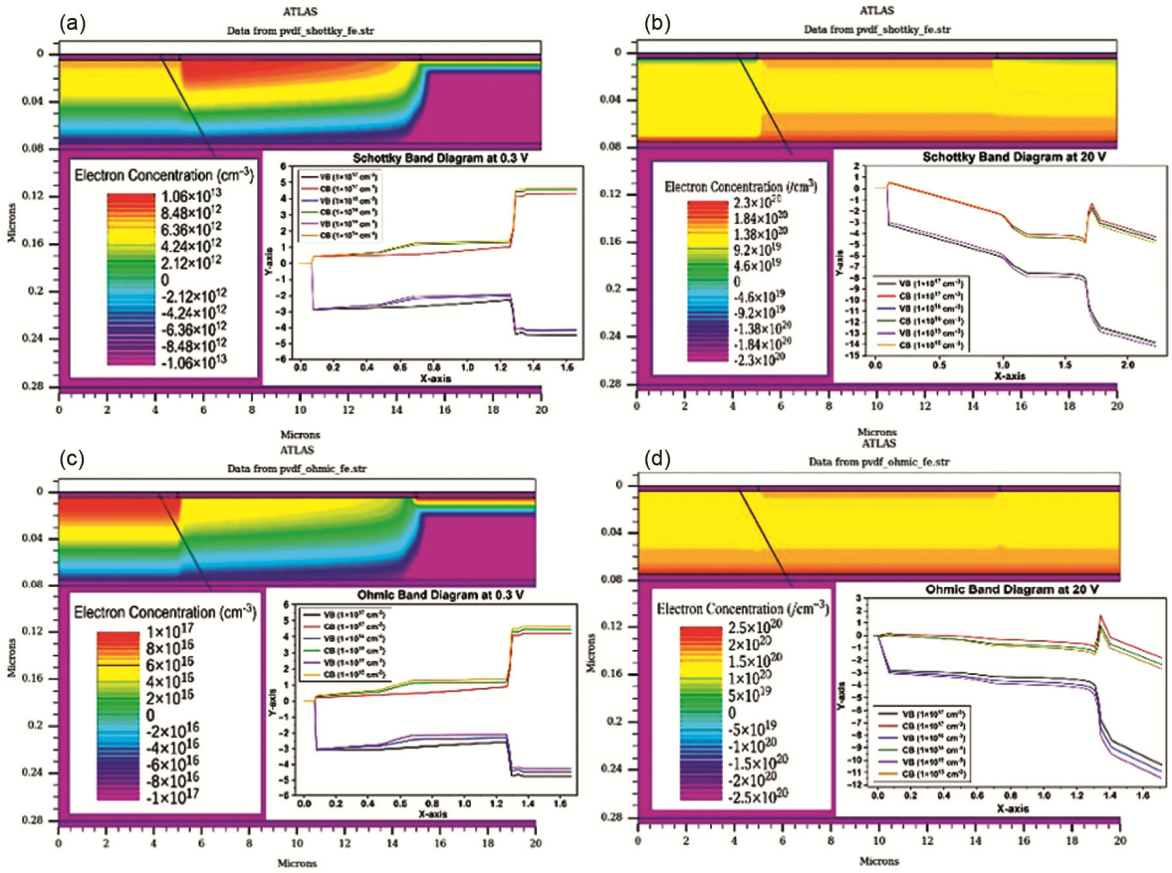

Fig. 4 — Electron concentration distribution and Energy Band Diagram (shown in inset) in ZnO/PVDF FeTFT at a ZnO electron concentration of 1×10^{17} cm^{-3}: (a) Schottky contact device at Vg=0.3V, (b) Schottky contact device at Vg = 20V, (c) Ohmic contact device at Vg = 0.3V, (d) Ohmic contact device at Vg = 20V

ZnO electron concentration of 1×10^{17} cm^{-3}. At a low gate bias of Vg = 0.3 V, the bottom gate electric field is relatively weak, resulting in only a weak accumulation layer near the ZnO/PVDF interface in the Ohmic contact device. The efficient carrier injection from the Ohmic source enables a small number of electrons to accumulate at the interface, representing the initial stage of channel formation. On the other hand, because of the Schottky barrier, there is partial depletion in the channel region which causes limited carrier injection, the Schottky contact device shows lower electron concentration near to the source side.

As the gate bias increases to Vg=20 V, the stronger vertical electric field significantly enhances electron accumulation at the ZnO/PVDF interface in both devices. However, the Ohmic contact device displays a higher and more uniform carrier distribution along the channel due to efficient carrier injection from the source. This reduced carrier availability leads to weaker electrostatic screening of ferroelectric polarization charges, allowing stronger modulation of the channel potential. Consequently, the threshold voltage shift becomes larger, resulting in an enhanced memory window in the Schottky contact device compared to the Ohmic contact device. Further the observed phenomena can be verified through energy band diagram extracted under the same conditions as that of electron density contours by taking diagonal cut across the source-channel-oxide regions. The Pd/ZnO interface in the Schottky contact device establishes a finite energy barrier that limits electron injection into the ZnO channel. At low gate bias (Fig. 4 (a) inset), the conduction band adjacent to the source stays comparatively elevated, leading to partial depletion and decreased electron concentration at the PVDF/ZnO interface. Despite elevated gate bias (Fig. 4 (b) inset), the conduction band exhibits downward bending due to gate-induced accumulation; nonetheless, the Schottky barrier still partially restricts carrier injection, especially at reduced ZnO electron concentrations. As a result, the electrostatic screening of ferroelectric polarization charges is less, facilitating more penetration of the polarization-induced electric field into the channel and resulting in

a more substantial modification of the channel potential and threshold voltage, thus widening the memory window. Conversely, the Ohmic contact device exhibits relatively uniform band profiles adjacent to the contacts (Fig. 4 (c) inset), with an insignificant injection barrier, facilitating effective electron injection into the ZnO channel even at minimal gate bias. At elevated gate bias (Fig. 4 (d) inset), the channel demonstrates significant electron buildup and a more homogeneous carrier distribution throughout the channel region. The augmented carrier availability effectively filters the ferroelectric polarization charges at the PVDF/ZnO interface, thus mitigating polarization-induced band modulation and diminishing the threshold voltage shift between the two polarization states. The Ohmic contact device demonstrates a markedly reduced memory window with minimal dependence on ZnO carrier concentration in contrast to the Schottky contact device.

4 Conclusion

This study demonstrates clearly that the nature of source/drain contact plays a very important role in determining the memory performances of ZnO/PVDF ferroelectric TFTs. It was noted that the memory window of devices with Schottky contacts is significantly larger about 2.86 V to 3.69 V, compared to that of the Ohmic contact devices about 0.2 V, almost independent of the carrier concentration. The key distinction between these two contact types is the way each type regulates the carrier injection and polarization screening. In Schottky contact devices, the energy barrier present restricts the injection of carriers into the channel. It is observed that, the carrier concentration close to the interface is lower, resulting in weaker screening of the ferroelectric polarization charges. Consequently, the polarization is better able to modulate the channel potential, leading to a greater change in threshold voltage and causing, an expanded memory window. This is even more pronounced with lower levels of doping in which the depletion region is extended and the polarization effect reaches even deeper into the semiconductor. Ohmic contacts in contrast permit free movement of the carriers into the channel. This causes an increase in the concentration of the carrier that strongly screens the polarization charges. As a result of this high screening, the polarization influence on the channel potential is negligible, and the threshold voltage shift decreases, as well as the memory window.

Overall, these findings indicate that controlling the contact type and carrier concentration is very important for designing high performance ferroelectric memory devices. Specifically, one possible solution is to use Schottky contacts to achieve a higher memory window by decreasing carrier screening and enabling higher control of polarization of the channel.

Acknowledgement

The authors would like to acknowledge the project funding received from the Board for Research in Nuclear Sciences (BRNS), Department of Atomic Energy (DAE), under Sanction No. 59/14/10/2023/12353 and Research Facilities Developed through DST Fund for Improvement of Science and Technology Infrastructure (FIST) under Grant SR/FST/ETI-411/2016. The authors also acknowledge the financial support provided by the Department of Science and Technology (DST) under the Promotion of University Research and Scientific Excellence (PURSE) scheme with Sanction No. SR/PURSE/2024/350 (TPN-105965). Additionally, the authors acknowledge the Research Initiation Grant (No. PEC/DSRIC/54) received from Punjab Engineering College (Deemed to be University), Chandigarh.

References

1 Yan A Z, Wang C L, Yan J L, Wang Z Z, Zhang E Y & Dong Y, *Adv Funct Mater*, 34 (2024) 2304409.

2 Acharya V, Agarwal K & Mondal S, *Mater Res Express*, 10 (2023) 082002.

3 Ozgur U, Alivov Y I & Liu C, *J Appl Phys*, 98 (2005) 041301.

4 Natu K, Laad M, Ghule B & Shalu A, *J Appl Phys*, 134 (2023) 190701.

5 Nomura K, Ohta H & Takagi A, *Nature*, 432 (2004) 488.

6 Jiao H, Wang X, Wu S, Chen Y, Chu J & Wang J, *Appl Phys Rev*, 10 (2023) 011310.

7 Rodriguez-Davila R A, Chapman R A, Bolshakov P, Young C D & Quevedo-Lopez M*, Microelectron Eng*, 217 (2019) 111114.

8 Vyas S, Dwivedi A D D & Dwivedi R, *Superlattices Microstruct*, 120 (2018) 223.

9 Mulaosmanovic H, Breyer E T, Dünkel S, Beyer S, Mikolajick T & Slesazeck S, *Nanotechnol*, 32 (2021) 502002.

10 Miller S L & McWhorter P J, *J Appl Phys*, 72 (1992) 5999.

11 Nalwa H S, *Ferroelectric Polymers: Chemistry, Physics, and Applications,* (Marcel Dekker, New York), 1995.

12 Lovinger A J, *Sci*, 220 (1983) 1115.

13 Park C H, Lee K H & Lee B H, *J Mater Chem*, 20 (2010) 2638.

14 Hoffman J, Pan X, Reiner J, Walker F, Han J, Ahn C & Ma T, *Adv Mater*, 22 (2010) 2957.

15 Dawber M, Rabe K M & Scott J F, *Rev Mod Phys*, 77 (2005) 1083.
16 Junquera J & Ghosez P, *Nature*, 422 (2003) 506.
17 Cheng G, Feng P X L & Guo J, *J Appl Phys*, 136 (2024) 154502.
18 Thesberg M, Obukhova T & Deleruyelle D, *IEEE Trans Electron Devices*, 71 (2024) 6686.
19 Sharma D K & Kumar V, *Memories Mater Devices Circuits Syst*, 7 (2024) 100096.
20 Sze S M & Ng K K, *Physics of Semiconductor Devices,* (John Wiley & Sons, Hoboken, NJ), 3rd Edn, 2007.
21 Tagantsev A K, Vaideeswaran K, Vakhrushev S B, *et al*, *Nat Commun*, 4 (2013) 2229.
22 Sharma D K, Khosla R & Sharma S K, *Solid State Electron*, 111 (2015) 42.
23 Zubko P, *Annu Rev Condens Matter Phys*, 2 (2011) 141.
24 Hoffmann M, *et al*, *Nature*, 565 (2019) 464.
25 Selberherr S, *Analysis and Simulation of Semiconductor Devices*, (Springer-Verlag, Vienna), 1984.
26 Silvaco Inc, *ATLAS Device Simulation Software User's Manual*, (Santa Clara, CA, USA), 2024.